

The Eurasia Proceedings of Science, Technology, Engineering & Mathematics (EPSTEM), 2022

Volume 17, Pages 69-82

ICRETS 2022: International Conference on Research in Engineering, Technology and Science

Efficient Decolorization of Anionic Dye (Methyl Blue) by Natural-Based Biosorbent (nano-Magnetic *Sophora Japonica* Fruit Seed Biochar)

Okan BAYRAM

Suleyman Demirel University

Elif KOKSAL

Suleyman Demirel University

Emel MORAL

Suleyman Demirel University

Fethiye GODE

Suleyman Demirel University

Erol PEHLIVAN

Konya Technical University

Abstract: Today, various methods are used to remove the dye pollution in the increasing water. Adsorption is a fast and effective method that has been used since the past. The value of the obtained adsorption capacity varies according to the type of biosorbent material used. The seeds of the fruit of *Sophora Japonica* (SJfs), a tree commonly found in nature, were pyrolyzed at 450°C to produce biochar (SJfsB) in this study. Iron nanoparticles were immobilized into the SJfsB structure to form a more active biosorbent matrix. The obtained SJfsB and nM-SJfsB were used in the removal of methyl blue, an anionic dye. SJfsB and nM-SJfsB used for dye removal were characterized by FT-IR and SEM instruments. The obtained results revealed that the adsorption process occurred in the pseudo-second-order and was consistent with the Langmuir model. The maximum adsorption capacity for MB removal was 434.783 mg/g for nM-SJfsB and 76.923 mg/g for SJfsB, respectively.

Keywords: Nanomagnetic-*Sophora Japonica* fruits seed biochar, Methyl blue, isotherm, kinetics

Introduction

Water pollution in the world has become a serious environmental problem that has gained importance with the development of many industries. Clean, drinkable water resources are gradually decreasing. Most industrial and domestic processes produce wastewater containing toxic substances (Amari et al. 2019). Pollutants that threaten the environment and human health, such as dyes and heavy metals, are often mixed with industrial wastewater and water sources in nature. Many industries such as cosmetics, leather, paper, textiles use dyes, and non-biodegradable dyes in these areas that use large amounts of water harm the environment with wastewater (Jawad et al. 2020). Dyes cause color pollution in water even at low concentrations, and this pollution delays photosynthesis by preventing light transmission. According to their ionic structure, dyes are divided into three as non-ionic, cationic and anionic dyes. Methyl blue is an anionic dye in the triphenylmethane group (Mouni et al. 2018). The treatment of wastewater and the use of purified water in industrial processes are gaining importance today. Many physical and chemical processes are applied for water purification. To treat dye-contaminated wastewater, various chemical, biological, and physical methods such as biodegradation, membrane filtration, ion exchange, electrochemical oxidation, and adsorption are used and many of them are

- This is an Open Access article distributed under the terms of the Creative Commons Attribution-Noncommercial 4.0 Unported License, permitting all non-commercial use, distribution, and reproduction in any medium, provided the original work is properly cited.

- Selection and peer-review under responsibility of the Organizing Committee of the Conference

costly (Arunachalam et al. 2018). Adsorption is one of the most effective and simple methods and it is used to detoxify and purify wastewater by removing its color and odor (Mohammed et al. 2022).

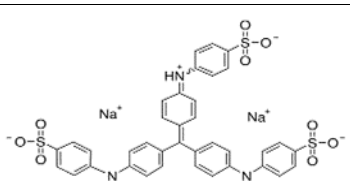
Adsorption occurs as a result of the formation of chemical and physical bonds between a porous solid surface and a liquid phase (Al-Ghouti & Da'ana, 2020). Biomass, agricultural wastes and natural minerals are at the forefront of environmentally friendly, low cost, easily available, high capacity, renewable biosorbents that do not form harmful by-products. Adsorption rate and selectivity are the most important properties of biosorbents. Researches on high selectivity biosorbents with fast adsorption and desorption rates are continuing (Kadhom et al. 2020). Biomass from plants contains oxygen-rich functional groups such as hydroxyl and carboxyl. The surface properties and adsorption capacity of these carbon-containing biosorbents are improved by chemical activation method (Jawad et al. 2020). As the specific surface area, pore volume, and surface chemical functional groups increase and the pore size decreases, the adsorption capacity of biosorbents increases. Biochar is obtained by pyrolysis of biomass in the presence of low oxygen. Surface area and porosity are two important physical and chemical properties of biochar. Biochar is rich in carbon content. It has a stable structure, large surface area and cation exchange capacity. Biochar is an biosorbent widely used to remove organic pollutants, toxic metals from industrial wastewater, agricultural wastewater, municipal wastewater (Wang & Wang 2019). Nanomaterials have been employed as a feasible choice of pollutant removal processes due to their unique qualities such as good recovery and high specific surface area. To protect human health and the natural environment, there is a need for nanobiosorbent materials to remove dyes from industrial wastes. The morphological and chemical properties of biological wastes can be enhanced by a wide variety of modification procedures (Bayram et al. 2022). One of them involves the inclusion of the magnetic form of nanomaterials matching the original structure. As biosorbents for dye removal, magnetically sensitive inexpensive biological materials were used. Recently, metals such as iron and their oxides have been used to obtain magnetic biochar. We created a magnetically modified biosorbent (nM-SJfsB) as a low-cost biosorbent for the removal of organic pollutants from an aqueous system in this study. SJfsB and nM-SJfsB were investigated and characterized for the removal of MB as anionic dye.

Materials and methods

Reagents and Instrumentation

The chemical materials ($\text{FeSO}_4 \cdot 7\text{H}_2\text{O}$, $\text{FeCl}_3 \cdot 6\text{H}_2\text{O}$, NaOH , HCl) used were obtained from Merck Company. Methyl blue (MB) was provided from Isolab Company. A 0.05 M HCl and 0.05 M NaOH solution was used to adjust the pH of the solutions. Table 1 shows the chemical formula, properties, and structures of MB.

Table 1. Some properties of methyl blue dye

Name	Molecular Formula	Molecular Weight	λ_{nm}	2D Structure
Methyl blue	$\text{C}_{37}\text{H}_{27}\text{N}_3\text{Na}_2\text{O}_9\text{S}_3$	799.81 g/mol	595-605 nm	

The samples for the FT-IR measurements were prepared using the KBr technique and peaks were recorded by Perkin Elmer Spectrum BX FT-IR spectrometer. The SEM FEI QUANTA 250 FEG was used for SEM images of the produced biosorbents.

Preparation methods

Wavelength Scan

In the wavelength scan, the highest absorbance value was measured at 600 nm. The wavelength scan for methyl blue is shown in Figure 1.

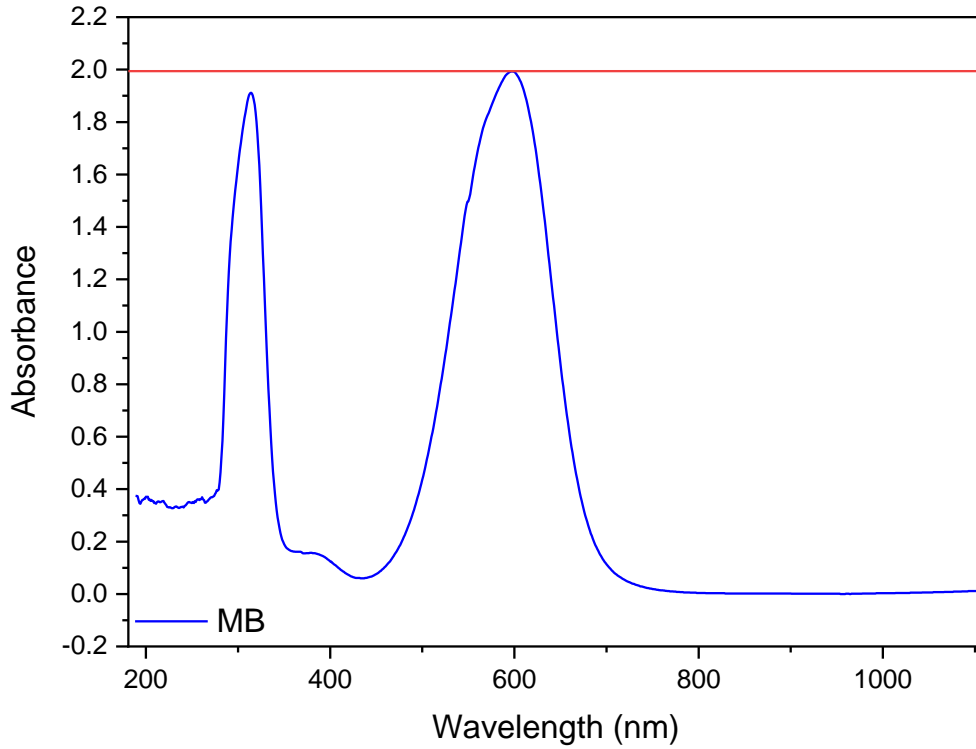


Figure 1. Wavelength of methyl blue

Preparation of Biochar (SJfsB)

SJfs were burned for 4.30 hours at 450 °C in a Carbolite ELF 11/6B brand muffle furnace. The produced SJfsB biochar and modified nM-SJfsB were used in the adsorption experiments.

Preparation of the nM-SJfsB

SJ seeds were cleaned and stored at room temperature for one day. It was then dried again for one more day at 60 °C. The co-precipitation method, which had previously been described in the literature, was used to prepare nM-SJfsB (Fig. 1) (Song et al. 2022). A volumetric flask was filled with 10 g of dried biosorbent. $FeCl_3 \cdot 6H_2O$ (1 M, 25 mL) and $FeSO_4 \cdot 7H_2O$ (1 M, 25 mL) solutions were added to a reactor containing 100 mL pure water, and the mixture was stirred at room temperature for one hour to dissolve the iron salt completely. After adding the biochar, the solution was stirred for another 30 minutes. The bottle is then filled with a 30% ammonia solution, which is added drop by drop to adjust the pH of the slurry, and the resulting yellow solution quickly turns into black precipitates. A color change revealed the production of the nM-SJfsB. The nM-SJfsB was filtered using a vacuum. The black precipitates were washed several times with deionized water and dried in an oven at 50 °C for one day after being separated from the solution phase using an external permanent magnet. For the adsorption experiments, the nM-SJfsB was stored in desiccator. The reactions that occur during the generation of nM-SJfsB are depicted below (Zhao et al. 2022):



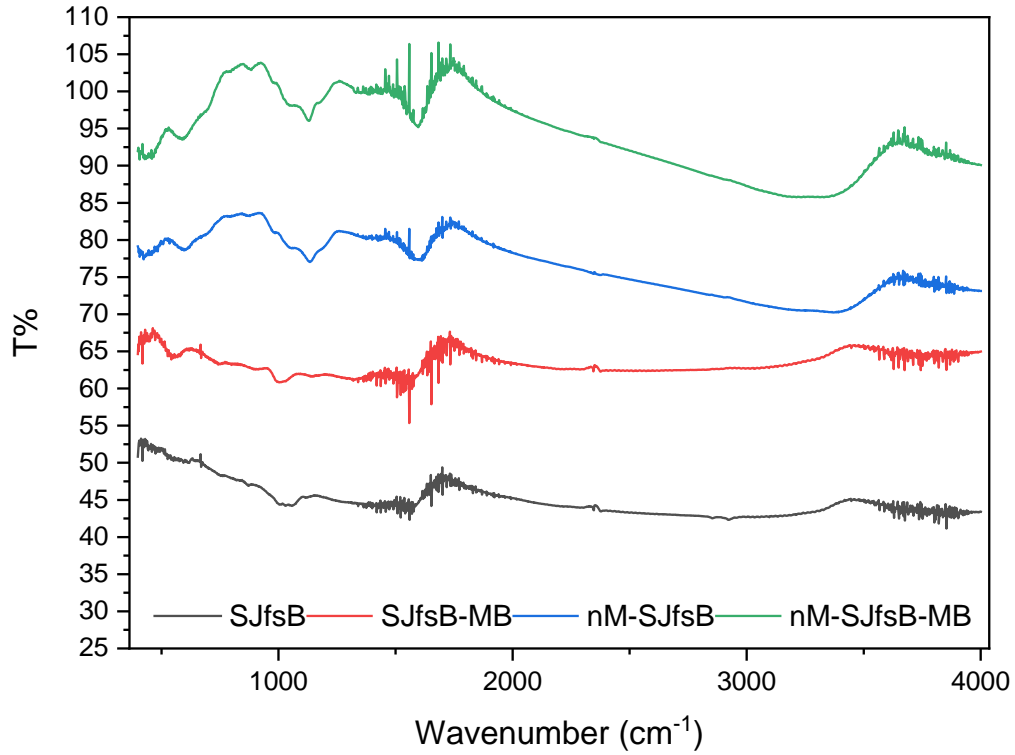


Figure 2. The FT-IR spectral characteristics of SJfsB, SJfsB-MB, nM-SJfsB and nM-SJfsB-MB

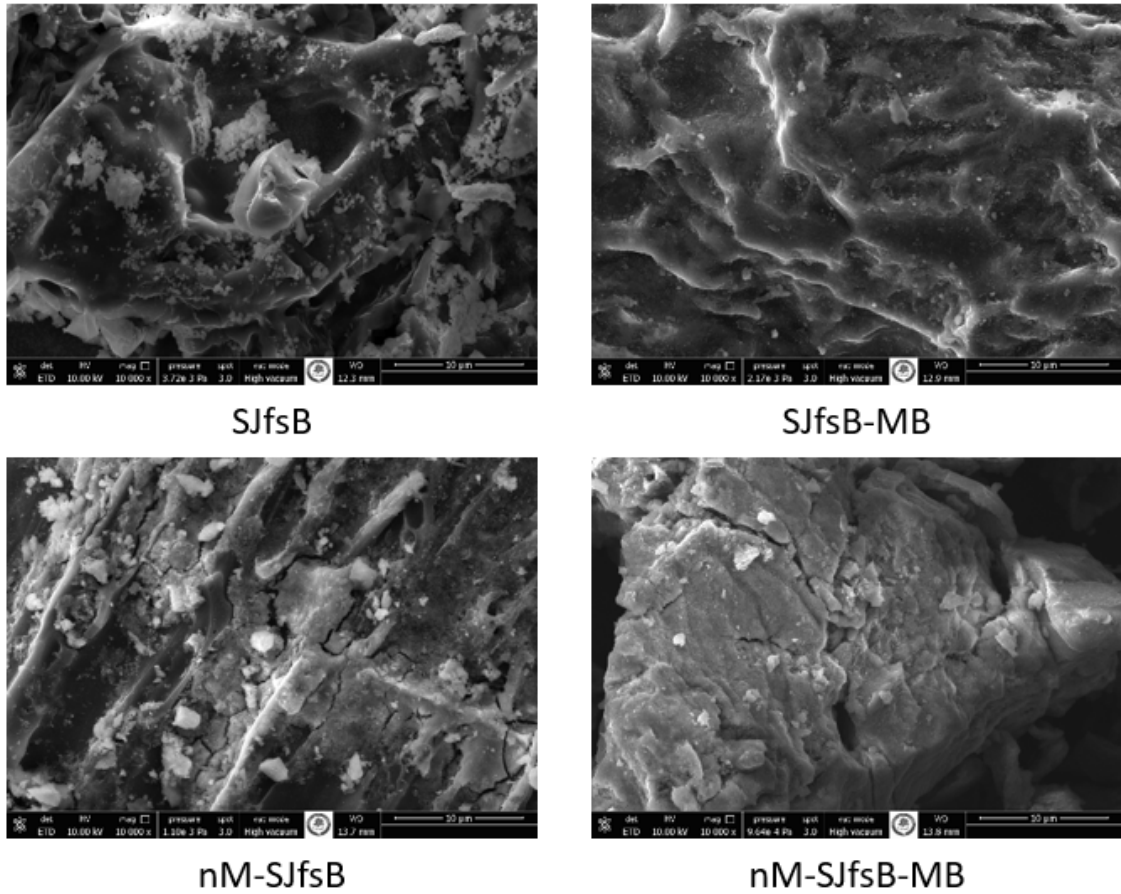


Figure 3. SEM images of SJfsB and nM-SJfsB before and after MB removal

FT-IR spectra for SJfsB, nM-SJfsB and SJfsB, MB adsorbed on nM-SJfsB were analyzed FT-IR spectrometer (in the infrared region of 4000–400 cm^{-1}). FT-IR spectroscopy was used to observe the chemical structures of SJfsB and chemically modified nM-SJfsB and to determine their functional groups. The spectra are given in Figure 3. When the spectra were examined, broadbands were observed at approximately 3516 cm^{-1} for SJfsB and 3583 cm^{-1} for nM-SJfsB. These bands correspond to the OH stretching vibration. Similar bands were observed in the FT-IR spectra of nM-SJfsB-MB around 3584 cm^{-1} (Bayram et al. 2022). The bands seen around 2989 cm^{-1} in the spectra in Figure 3. correspond to the C–H stretching vibrations in the structure. Similar band was seen around 3010 cm^{-1} in modified nM-SJfsB, nM-SJfsB-MB spectra. The FT-IR spectrum showed that nM-SJfsB's generally consisted of functional groups such as alcohol, phenol, carboxylic groups (O–H groups, C=O and –C–O bonds). The formation of these groups is thought to be due to complexation reactions with MB (Khan et al. 2022; Deng et al. 2022). Stretching vibrations of the C=O bond in the spectra of SJfsB (1774 cm^{-1}) and nM-SJfsB (1757 cm^{-1}) were observed in similar bands in the FT-IR spectra of SJfsB-MB and nM-SJfsB-MBs. This result demonstrated that both SJfsB and chemically modified nM- SJfsBs interacted with dyes as expected. The bands at 786 and 654 cm^{-1} in nM-SJs have been assigned to Fe-O vibrational bonds, confirming the presence of Fe components (Bayram et al. 2022; Wang et al. 2018). The changes and intensities in the bands observed following MB adsorption in nM- SJfsBs suggested that they could be indicative of MB adsorption with functional groups present in nM- SJfsBs.

The surface morphology of both SJfsB and nM-SJfsB was investigated using scanning electron microscopy (SEM) before and after dye adsorption. SEM images were taken on a Quanta FEG250 (Thermo Fisher Scientific) brand device and a magnification of 10000x was used. SEM examination at various magnifications revealed morphological changes before and after MB biosorbent. Figure 4 depicts the surface morphology results from SEM images, and the surface of SJfsB was discovered to be very porous and amorphous. These spherical granules have a brilliant, noticeable appearance. SEM analysis of nM-SJfsB revealed a wide range of voids on the surface that can be beneficial for MB removal, as well as a significant change in the structure of the biosorbent (Bayram et al. 2022).

Adsorption experiments of MB with the biosorbents

The batch method was used to investigate dye adsorption on the nM-SJfsB with different parameters such as temperature, concentration, pH, and time. To confirm the equilibrium at 25 °C, the following MB batch adsorption experiments were designed: The saturation of biosorbent by MB was investigated using 0.2 g dosages of SJfsBs and nM-SJfsB in solutions containing 200 mg/L MB. The beaker was removed from the shaker and was placed in an incubator shaker (250 rpm) at 25 °C for different contact times (15 minutes, 30 minutes, 60 minutes, 90 minutes, 120 minutes, 180 minutes, and 240 minutes), and then removed from the shaker. The effect of SJfsB and nM-SJfsB biosorbent amount on MB removal was tested by mixing 200 mg/L MB solutions with the certain amount of the biosorbent for 60 minutes. In each vessel, the amount of nM-SJfsB in the dye solution was 0.05 g, 0.1 g, 0.2 g, 0.5 g and 0.75 g. The pH of the solution phase was adjusted from 2 to 9 by including 0.2 g of nM-SJfsB in serious beakers containing 200 mg/L of MB solution. Different starting concentrations of MB (25 mg/L-300 mg/L) were investigated at a stationary pH value of the dye solution. The experiments were repeated to ensure the data's dependability and accuracy. Following the adsorption process, nM-SJfsB was separated from the solution medium with a magnetic bar, and the remaining dye concentration was determined with a UV-Vis spectrometer set to 600 nm for MB. The following equation was used to calculate the adsorption capacity (q_e) of biosorbents. (Eq. (3 and 4)):

$$q_e = \frac{(C_o - C_e)V}{W} \quad (3)$$

where C_o (mg/L) is initial dye concentration and C_e (mg/L) is equilibrium dye concentration. V (L) is the volume of the dye solution and m (g) is the amount of biosorbent.

The color removal efficiency was calculated using the following formula.

$$Colour(\%) = \frac{100(C_o - C_e)}{C_o} \quad (4)$$

where C_o is initial MB concentration and C_e is the equilibrium MB concentration. The volume of the solution is denoted by V (mL), and the amount of SJfsBs and nM-SJfsB is denoted by W (g). Eq. (3) was used to calculate the q_e (mg/g) of the SJfsBs and nM-SJfsB. In an equilibrium study, each trial is repeated twice.

Results and Discussion

Effect of different parameters on MB removal

Effect of contact time

0.2 g biosorbent was added to 30 mL of the prepared 200 mg/L MB (pH: ~5.0-5.5) solution. The dyes were adsorbed at various times ranging from 15 to 240 minutes, and the effect of contact time on adsorption was investigated. Figure 5 depicts the effect of contact time on MB adsorption. Adsorption experiments measuring the effect of contact time revealed a slower phase in which MB adsorption began rapidly and tended to the horizontal asymptote in the first 30 minutes. Figure 5 shows that nM-SJfsB has significantly greater adsorption ability than SJfsB. The experiment found that 40-80 minutes of contact time was sufficient to achieve the biosorbent substance-MB equilibrium.

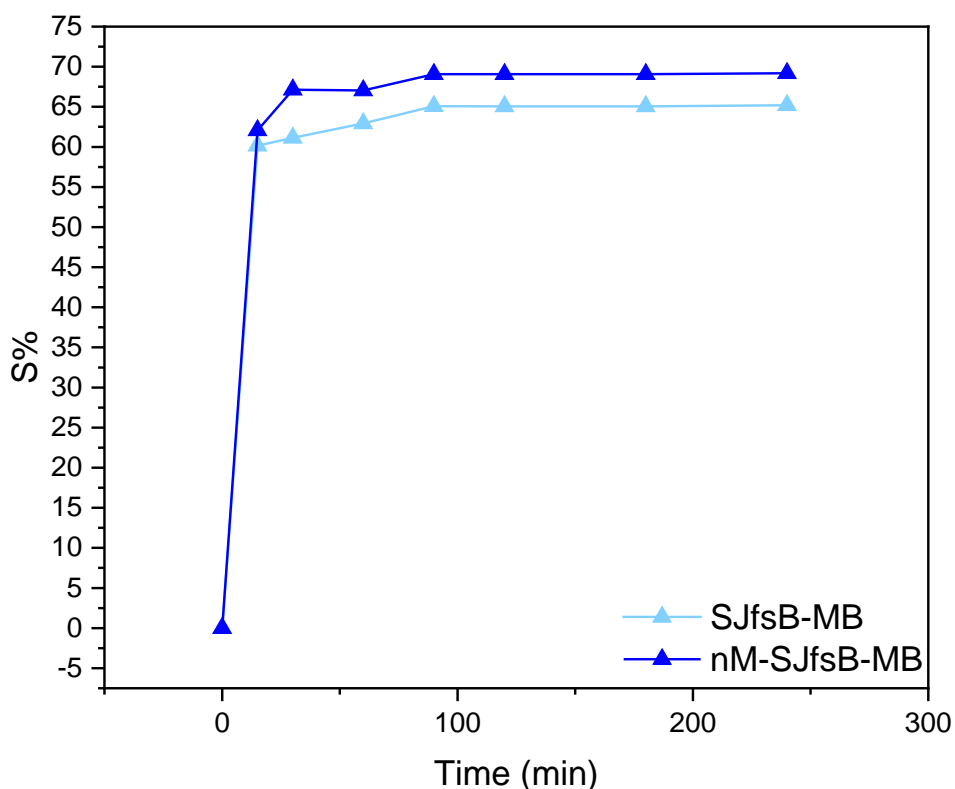


Figure 4. Effect of time change on adsorption (conditions: biosorbent amount: 0.2 g; concentration of dyes: 200 mg/L MB, temperature: 25 ± 1 °C, pH: solution pH 5.0–5.5 for MB; time: 30 min, 45 min, 60 min, 90 min, 120 min, 180 min, 240 min).

Effect of pH on Biosorption

The adsorption process is controlled by pH, which affects the surface charge of the biosorbent, the strength of ionization, the division of functional groups, the specification of the adsorbate, and the degree of ionization. Traditional biosorbents remove decolorization primarily through adsorption, and they may be effective if the concentration of dye in the solution is quite low. It is known that properties such as physical, mechanical, and chemical properties are effective in the interaction of dyes with biosorbent. In adsorption studies, the effect of pH is an important factor in the adhesion interactions of dye to the biosorbent surface. The adsorption of dyes is significantly affected by the surface charge on the biosorbent (nM-SJfsB). The pH is an effective factor in the ionization of MB and the chemical properties of nM-SJfsB in adsorption studies. The pH range of 5.0-5.5 provided the best dye adsorption for both biosorbents.

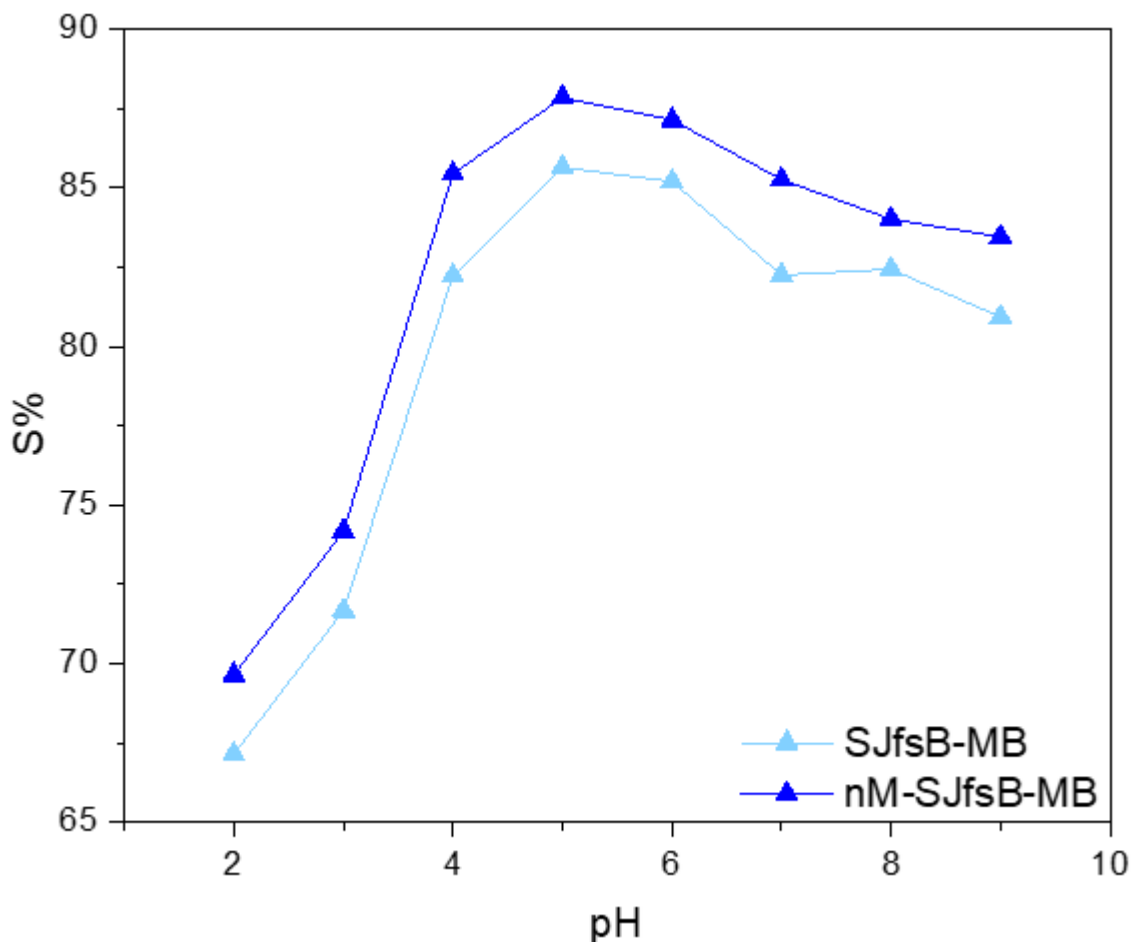


Figure 5. Effect of time change on adsorption (conditions: biosorbent amount: 0.2 g; concentration of dyes: 200 mg/L MB, temperature: 25 ± 1 °C, pH: solution pH 2.0–9.0 for MB; time: 60 min).

Effect of MB Initial Concentration (Adsorption Isotherms)

Adsorption isotherm models are used to explain the distribution of adsorbate molecules on the biosorbent surface when the solid and liquid phases are in equilibrium. Figure 7 shows the adsorption values obtained for equilibrium studies at various MB concentrations. Adsorption capacity SJfsBs and nM-SJfsB by changing the dye concentrations to 25 mg/L–300 mg/L were calculated. It indicates that the percent adsorption of MB reaches a horizontal equilibrium after the initial concentration of 300 mg/L. This is because MB saturation of active sites in SJfsBs and nM-SJfsB coats the surfaces of the biosorbents with sufficient dyes, causing the adsorption rate to slow down until equilibrium is reached. Over time, the surface of the biosorbents becomes saturated and thus the rate of adsorption slows down. Langmuir, Freundlich, Temkin, Dubinin and Radushkevich and Scathard isotherms were used to correlate experimental equilibrium adsorption data (Zhang et al. 2022, Jain et al. 2022). The isotherm equations and the obtained calculation results are shown in Table 2. Compared with other isotherms, Langmuir isotherm was found to be more suitable for dye adsorption. If the calculated R_L value is between 0 and 1, the sorption is considered sufficient. SJfsB and nM-SJfsB strongly absorbed MB dyes from the solution phase with R_L values ranging from 0.016 to 0.290 in our study (Table 2) (Bayram et al. 2022). For SJfsB and nM-SJfsB, the Langmuir isotherm model's high correlation coefficient range (R^2 : 0.949–0.979) is more suitable (Table 2). The results showed that the adsorption process occurred in the pseudo-second order, which was consistent with the Langmuir model. The maximum adsorption capacity for MB removal for SJfsB was 434.783 mg/g for nM-SJfsB and 76.923 mg/g for SJfsB, respectively. The Freundlich isotherm was used to predict the adsorption process occurring on the heterogeneous biosorbent surface (Giri et al., 2022). The K_f and n parameters of the Freundlich equation were calculated and the n values were found to be 1.257 for MB adsorption by nM-SJfsB and 1.658 for MB adsorption by SJfsBs. If n is between 1 and 10, adsorption is considered suitable. The Freundlich isotherm model calculated K_f values of 19,173 mg/g for SJfsB-MB and 17,721 mg/g for nM-SJfsB-MB.

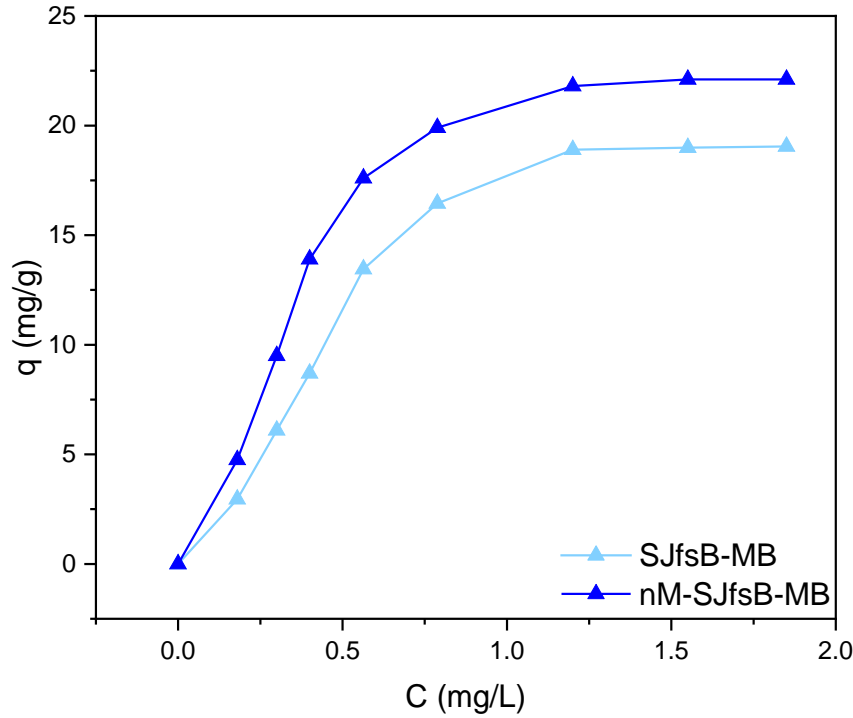


Figure 6. Effect of concentration change on adsorption (conditions: biosorbent amount: 0.2 g; concentration of dyes: 25 mg/L, 50 mg/L, 75 mg/L, 100 mg/L, 150 mg/L, 200 mg/L, 250 mg/L, 300 mg/L MB, temperature: 25 ± 1 °C, pH: solution pH 5.0–5.5 for MB; time: 60 min).

Table 2. Adsorption isotherm parameters and results

Equation	Eq. no.	Biosorbent	Dye	Parameters for dye			
Langmuir (1916)	$\frac{1}{q_e} = \frac{1}{K_L q_{max}} \times \frac{1}{C_e} + \frac{1}{q_{max}}$ (5)	SJfsB	MB	q_{max}	K_L	R^2	R_L
		nM-SJfsB	MB	76.923	0.405	0.929	0.047
Freundlich (1907)	$Log q_e = Log K_f + \frac{1}{n} Log C_e$ (6)	SJfsB	MB	434.78	0.049	0.949	0.290
		nM-SJfsB	MB	K_f	n	R^2	
Dubinin and Radushkevich (1947)	$ln q_e = ln q_m - \beta \epsilon^2$ (7)	SJfsB	MB	19.173	1.658	0.831	19.173
		nM-SJfsB	MB	17.721	1.257	0.899	17.721
Scatchard (1949)	$\frac{q_e}{C_e} = Q_s K_s - q_e K_s$ (8)	SJfsB	MB	X_m	K	E	R^2
		nM-SJfsB	MB	3.071	4×10^{-8}	4082.482	0.992
Temkin and Pyzhev (1940)	$q_e = B \ln K_T + B \ln C_e$ (9)	SJfsB	MB	2.582	3×10^{-8}	3535.533	0.984
		nM-SJfsB	MB	Q_s	K_s	R^2	
		SJfsB	MB	26.608	3.552	0.960	
		nM-SJfsB	MB	19.315	39.815	0.997	
		SJfsB	MB	BT	K_t	R^2	
		nM-SJfsB	MB	8.452	8.776	0.980	
		nM-SJfsB	MB	10.684	8.655	0.989	

Effect of SJfsB and nM-SJfsB dosage

In adsorption studies, the amount of nM-SJfsB that will provide maximum dye adsorption should be determined. Figure 8 shows the relationship between the amount of nM-SJfsB and its biosorption capacity. Between 0.05 g and 0.75 g of SJfsB and nM-SJfsB were added to the reactor bottles and 30 mL of 200 ppm MB was placed on it. At the end of 60 minutes of shaking, the optimal biosorbent amount was determined. Approximately 70.0% of MB could be removed with 0.2 g SJfsB and nM-SJfsB and further addition of biosorbents did not alter dye adsorption (Figure 8.), which quickly reached equilibrium. The high dye uptake could be attributed to the high adsorption displayed on the surface of the biosorbents. This could be due to the amorphous and porous structure of biosorbents (Chen et al. 2022, Liu et al. 2022). The optimum amount of biosorbent was determined in the equilibrium study to be 0.2 g. By increasing the amount of biosorbent, the biosorbent was able to have more surface contact area. As a result, the adsorption percentage increased. Aggregation of the biosorbent material may occur as the amount of biosorbent used in the experiments increases. As a result, the surface area is reduced. This was seen with 0.75 g of nM-SJfsb.

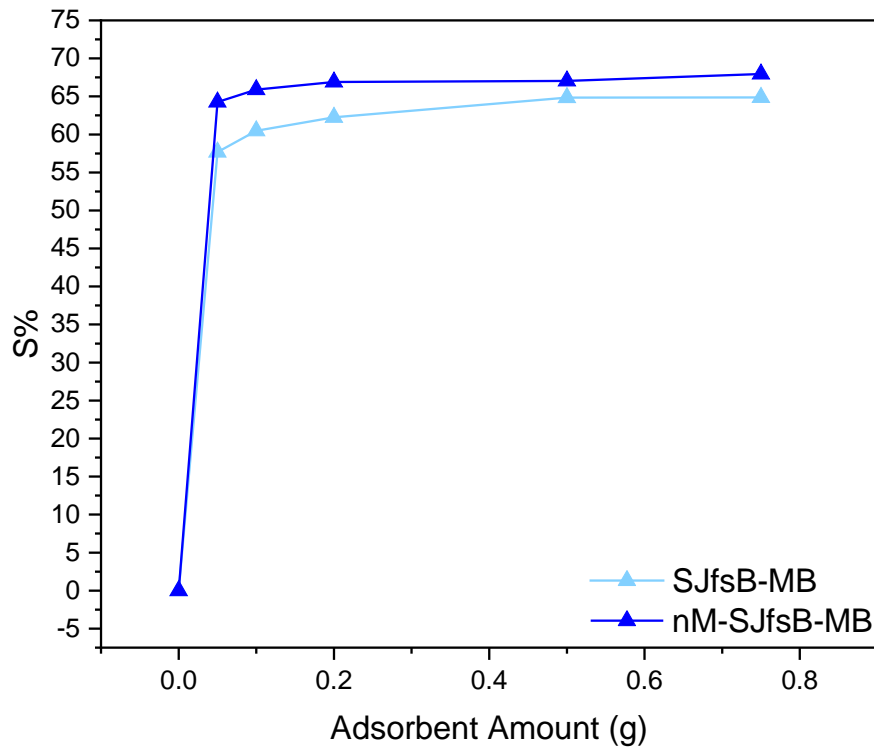


Figure 7. Effect of biosorbent amount change on adsorption (conditions: biosorbent amount: 0.05 g, 0.1 g, 0.2 g, 0.5 g, 0.75 g; concentration of dyes: 200 mg/L MB, temperature: 25 ± 1 °C, pH: solution pH 5.0–5.5 for MB; time: 60 min).

Kinetic Models

The many adsorptions kinetics, developed according to various physical and chemical conditions, are used to determine which mechanisms the adsorbed material fits during its adsorption onto the biosorbent surface. Adsorption kinetic modelling was used to explain dye transfer from solution phase to the solid phase (Huang et al. 2022, Srikaow et al. 2022), with the observed data fitted to pseudo-first-order and pseudo-second-order kinetic models. To determine the mechanism of retention of dyes on the surface of nM-SJFSB and to understand the speed control step, kinetic data were equipped with these kinetic models. The pseudo-first-order kinetic model and pseudo-second-order kinetic equations are written as follows (Eq. 10 and Eq. 11):

$$q_t = q_e(1 - e^{-k_1 t}) \tag{10}$$

$$\frac{1}{q_t} = \frac{1}{k_2 q_e^2} + \frac{1}{q_e t} \tag{11}$$

Table 3. Rate constants for the biosorption of MB with original and modified biosorbent (Pseudo-first-order kinetic equation and Pseudo-second-order kinetic equation)

	Sorbent	q_{e-cal} (mg/g)	k_1 (1/min)	q_{e-exp} (mg/g)	R^2
First Order	SJfsB	17.995	1.25×10^{-09}	20.036	0.955
	nM-SJfsB	18.013	1.25×10^{-08}	20.157	0.907
	Sorbent	q_{e-cal} (mg/g)	k_2 (g/mg. min.)	q_{e-exp} (mg/g)	R^2
Second Order	SJfsB	19.700	0.013	20.036	0.998
	nM-SJfsB	20.200	0.464	20.157	1.000

q_{e-cal} =calculated, q_{e-exp} =experimentally found)

The reaction order of dye adsorption on biosorbents was investigated. Table 3 shows the parameters of the kinetic models for MB adsorption. As shown in Table 3, the adsorption process for MB showed the pseudo-second-order rate model. Despite this, the calculated value (q_e) for the pseudo-second-order model deviated significantly less from the pseudo-first-order experimental data. The fact that the pseudo-second-order model has a higher R^2 value indicates that this model equation is more effective for adsorption kinetic studies (Yagnamurthy et al. 2022, Isik et al. 2022).

Thermodynamic Studies

The adsorption capacity of nM-SJfsB increased with increasing temperature of the system. This shows that the adsorption is endothermic. (Fig. 9). To determine the process, the following thermodynamic parameters must be considered: changes in standard enthalpy ΔH^0 and standard entropy ΔS^0 caused by the transfer of a unit mole of dye from solution to the biosorbent-liquid interface. Using the Van't Hoff equation, the values of ΔH^0 and ΔS^0 can be calculated from adsorption data at different temperatures (Saeed et al. 2022). Thermodynamic studies have been completed at various temperatures (25 °C, 35 °C, 45 °C, and 55 °C) and ΔH^0 , ΔS^0 and ΔG^0 values were calculated (Table 4.). In equilibrium studies, when the ambient temperature of the solution is raised from 25 °C up to 55 °C, the capacity of SJfsB decreased slightly, while the capacity of nM-SJfsB increased slightly. This is the situation that demonstrates a weakening or slight strengthening of the binding relationship between the dyes and biosorbent’s active sites (Kayalvizhi et al. 2022).

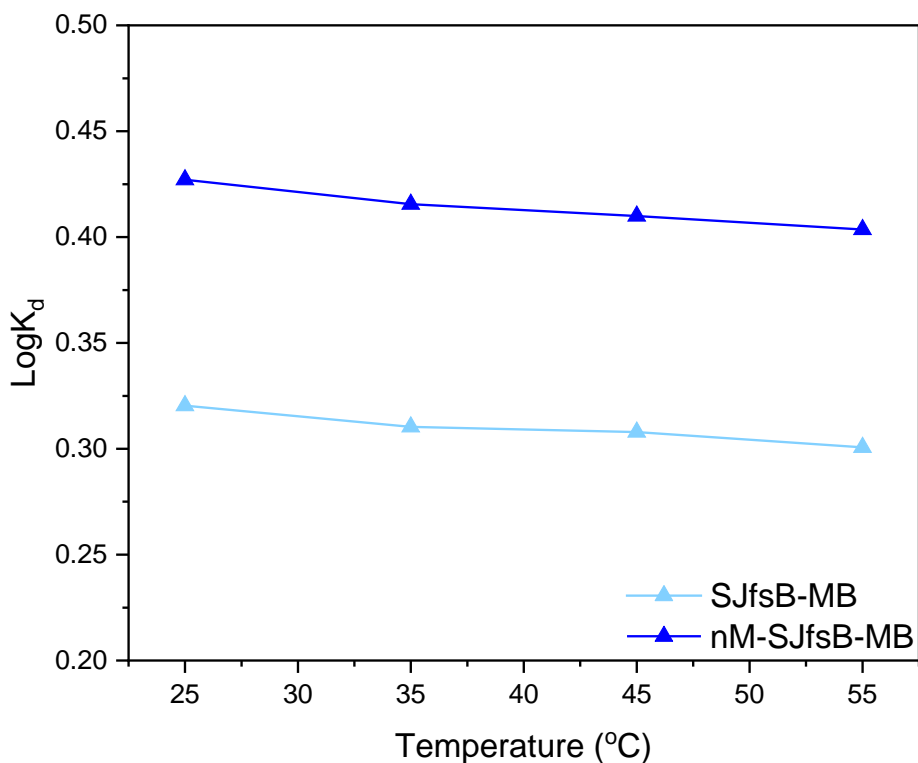


Figure 8. Effect of temperature change on adsorption (conditions: biosorbent amount: 0.2 g; concentration of dyes: 200 mg/L MB, temperature: 25 ± 1 °C, 35 ± 1 °C, 45 ± 1 °C, 55 ± 1 °C pH: solution pH 5.0–5.5 for MB; time: 60 min).

Table 4. Thermodynamic parameters for MB removal with SJfsB and nM-SJfsB

Dye	T(K)	ΔS° (kJmol ⁻¹)	ΔH° (kJmol ⁻¹)	ΔG° (kJmol ⁻¹)
SJfsB-MB	298.150	2.262	-1.147	-1.827
	308.150			-1.830
	318.150			-1.875
	328.150			-1.888
nM-SJfsB-MB	298.150	3.348	-1.431	-2.437
	308.150			-2.450
	318.150			-2.496
	328.150			-2.534

The equilibrium constant is calculated in relation to temperature change using the following equation (Eq 12, Eq 13):

$$\ln K_L = -\frac{\Delta H^{\circ}}{RT} + \frac{\Delta S^{\circ}}{R} \quad (12)$$

where, K_L equilibrium constant, T temperature (K); R, ideal gas constant. The changes in the free energy (ΔG° , kJ/mol) values were calculated from Equation (13).

$$\Delta G^{\circ} = \Delta H^{\circ} - T\Delta S^{\circ} \quad (13)$$

SJfsB-MB and nM-SJfsB-MB exothermic responses are indicated by negative ΔH° values. The positive ΔS° values indicates that the biosorbent-solution boundary is disordered during dye absorption of SJfsB-MB and nM-SJfsB-MB. Negative ΔG° values indicate that the adsorption technique is applicable, and that dye adsorption is self-executing and spontaneous. Adsorption processes were exothermic and spontaneous. Thermodynamic parameters indicate that physisorption is the primary mechanism of dye adsorption to SJfsB-MB, nM-SJfsB-MB.

Recycling and Reusability of nM-SJfsB

The adsorption process used in wastewater treatment is a simple, low-cost, and highly efficient method in which pollutants are absorbed on biosorbent surfaces, without by-products. The desorption of dyes is an important in the adsorption process. Considering whether biosorbents can be reused is important in determining the adsorption mechanism. In the experiment, 0.1 mol/L diluted HCl was used as a desorption agent to examine the reuse of biosorbents (Ghaedi et al. 2022, Wu et al. 2022). The biosorbent still has a high adsorption efficiency after three cycles (respectively 92.0 %, 91.2%, 90.1% removal). These good results show that biosorbents can be used to remove MB effectively.

Comparison of MB removal with different biosorbents reported in the literature

Table 5 compares the biosorption capacity of dyes to various biosorbents studied in the literature. Because of its unique properties, nM-SJfsB has a higher dye adsorption capacity than others. This previously unpublished biosorbent may be useful for removing dyes from aqueous solutions.

Table 5. Comparison of maximum biosorption capacities of literature results with our results for MB dyes

Types of biosorbents	Dye	Biosorption capacities (mg/g)	Reference
TPP-PP	MB	159.80	He et al. 2022
Na-BaLa ₄ Ti ₄ O ₁₅	MB	37.6	Chang et al. 2022
Zn-BaTiO ₃ /BaLa ₂ Ti ₃ O ₁₀	MB	33.0	Chang et al. 2022
BMNPs	MB	136	Wang et al. 2017
Nanoporous Carbon	MB	555.56	Han et al. 2018
ZnCo ₂ O ₄	MB	2400	Lin et al. 2018
SJfsB	MB	76.923	Present work
nM- SJfsB	MB	434.783	Present work

Conclusion

The adsorption efficiency of modified SJfsB in the removal of MB from the aqueous environment was investigated in this study. The results revealed that dye removal was sped up in the early stages of the biosorbent's contact with the dye, then increased and slowed when it reached equilibrium. The experiments were carried out over a period of 240 minutes. After examining the various dye concentration options, the MB was removed with high capacity by nM-SJfsB, and equilibrium was reached in a very short time, and the biosorbent efficiently adsorbed most of the dyes in the solution phase. The adsorption model fit to the Langmuir isotherm. The maximum adsorption capacity for SJfsB-MB was 76.923 mg/g, and the maximum adsorption capacity for nM-SJfsB was 434.783 mg/g. Negative ΔG^0 values calculated from thermodynamic studies indicated that the adsorption technique is applicable and dyes adsorption occur spontaneously. The biosorbents demonstrated reusability and a high adsorption capacity during the sequential adsorption cycle. This research demonstrates that the nM-SJfsB can be replaced with a green synthesis approach to create a biochar/nano iron composite with good dye removal capacity. The proposed nM-SJfsB provides a new solution for the long-term, cost-effective removal of harmful contaminants from toxic dyes. The results show that using a green synthesis approach to create nM-SJfsB is an effective way to improve the properties and potential practical applications of this nano-biosorbent for toxic dye environmental remediation.

Scientific Ethics Declaration

The authors declare that the scientific ethical and legal responsibility of this article published in EPSTEM journal belongs to the authors.

Acknowledgements or Notes

This article was presented as an oral presentation at the International Conference on Research in Engineering, Technology and Science (www.icrets.net) conference held in Baku/Azerbaijan on July 01-04, 2022.

References

- Al-Ghouti, M. A., & Da'ana, D. A. (2020). Guidelines for the use and interpretation of adsorption isotherm models: A review. *Journal of hazardous materials*, 393, 122383.
- Amari, A., Alalwan, B., Eldirderi, M. M., Mnif, W., & Rebah, F. B. (2019). Cactus material-based biosorbents for the removal of heavy metals and dyes: a review. *Materials Research Express*, 7(1), 012002.
- Arunachalam, A., Chaudhuri, R. G., Iype, E., & Prakash Kumar, B. G. (2018). Surface modification of date seeds (*Phoenix dactylifera*) using potassium hydroxide for wastewater treatment to remove azo dye. *Water Practice & Technology*, 13(4), 859-870.
- Bayram, O., Koksal, E., Gode, F., & Pehlivan, E. (2022). Decolorization of water through removal of methylene blue and malachite green on biodegradable magnetic *Bauhinia variagata* fruits. *International Journal of Phytoremediation*, 24(3), 311-323.
- Chang, A. L., Nguyen, B. S., Nguyen, V. H., & Hu, C. (2022). Adsorption kinetics of methyl blue using metal-modified barium lanthanum titanate as an effective absorbent. *Materials Chemistry and Physics*, 276, 125363.
- Chen, W. H., Hoang, A. T., Nižetić, S., Pandey, A., Cheng, C. K., Luque, R., ... & Nguyen, X. P. (2022). Biomass-derived biochar: From production to application in removing heavy metal-contaminated water. *Process Safety and Environmental Protection*, 160, 704-733.
- Deng, Z., Gu, S., Cheng, H., Xing, D., Twagirayezu, G., Wang, X., ... & Mao, M. (2022). Removal of Phosphate from Aqueous Solution by Zeolite-Biochar Composite: Adsorption Performance and Regulation Mechanism. *Applied Sciences*, 12(11), 5334.
- Dubin, M. M. (1947). The equation of the characteristic curve of activated charcoal. In *Dokl. Akad. Nauk. SSSR*. (Vol. 55, pp. 327-329).
- Freundlich, H. (1907). Über die adsorption in losungen. *Zeitschrift für physikalische Chemie*, 57(1), 385-470.
- Ghaedi, S., Seifpanahi-Shabani, K., & Sillanpää, M. (2022). Waste-to-Resource: New application of modified mine silicate waste to remove Pb²⁺ ion and methylene blue dye, adsorption properties, mechanism of action and recycling. *Chemosphere*, 292, 133412.

- Giri, B. S., Sonwani, R. K., Varjani, S., Chaurasia, D., Varadavenkatesan, T., Chaturvedi, P., ... & Pandey, A. (2022). Highly efficient bio-adsorption of Malachite green using Chinese Fan-Palm Biochar (*Livistona chinensis*). *Chemosphere*, 287, 132282.
- Han, X., Wang, H., & Zhang, L. (2018). Efficient removal of methyl blue using nanoporous carbon from the waste biomass. *Water, Air, & Soil Pollution*, 229(2), 1-10.
- He, Y., Bao, W., Hua, Y., Guo, Z., Fu, X., Na, B., ... & Liu, H. (2022). Efficient adsorption of methyl orange and methyl blue dyes by a novel triptycene-based hyper-crosslinked porous polymer. *RSC Advances*, 12(9), 5587-5594.
- Huang, H., Zheng, Y., Wei, D., Yang, G., Peng, X., Fan, L., ... & Zhou, Y. (2022). Efficient removal of pefloxacin from aqueous solution by acid-alkali modified sludge-based biochar: adsorption kinetics, isotherm, thermodynamics, and mechanism. *Environmental Science and Pollution Research*, 29(28), 43201-43211.
- Isik, Z., Saleh, M., M'barek, I., Yabalak, E., Dizge, N., & Deepanraj, B. (2022). Investigation of the adsorption performance of cationic and anionic dyes using hydrocharred waste human hair. *Biomass Conversion and Biorefinery*, 1-14.
- Jain, M., Khan, S. A., Sahoo, A., Dubey, P., Pant, K. K., Ziora, Z. M., & Blaskovich, M. A. (2022). Statistical evaluation of cow-dung derived activated biochar for phenol adsorption: Adsorption isotherms, kinetics, and thermodynamic studies. *Bioresource Technology*, 352, 127030.
- Jawad, A. H., Abdulhameed, A. S., & Mastuli, M. S. (2020). Acid-factionalized biomass material for methylene blue dye removal: a comprehensive adsorption and mechanism study. *Journal of Taibah University for Science*, 14(1), 305-313.
- Kadhom, M., Albayati, N., Alalwan, H., & Al-Furaiji, M. (2020). Removal of dyes by agricultural waste. *Sustainable Chemistry and Pharmacy*, 16, 100259.
- Kayalvizhi, K., Alhaji, N. M. I., Saravanakumar, D., Mohamed, S. B., Kaviyarasu, K., Ayeshamariam, A., ... & Elshikh, M. S. (2022). Adsorption of copper and nickel by using sawdust chitosan nanocomposite beads—A kinetic and thermodynamic study. *Environmental Research*, 203, 111814.
- Khan, B. A., Ahmad, M., Iqbal, S., Bolan, N., Zubair, S., Shafique, M. A., & Shah, A. (2022). Effectiveness of the engineered pinecone-derived biochar for the removal of fluoride from water. *Environmental Research*, 113540.
- Langmuir, I. (1916). The constitution and fundamental properties of solids and liquids. Part I. Solids. *Journal of the American chemical society*, 38(11), 2221-2295.
- Lin, K., Qin, M., Geng, X., Wang, L., & Wu, H. (2018). ZnCo₂O₄ nanorods as a novel class of high-performance biosorbent for removal of methyl blue. *Advanced Powder Technology*, 29(8), 1933-1939.
- Liu, Z., Zhen, F., Zhang, Q., Qian, X., Li, W., Sun, Y., ... & Qu, B. (2022). Nanoporous biochar with high specific surface area based on rice straw digestion residue for efficient adsorption of mercury ion from water. *Bioresource Technology*, 127471.
- Mohammed Ali, N. S., Alalwan, H. A., Alminshid, A. H., & Mohammed, M. M. (2022). Synthesis and Characterization of Fe₃O₄-SiO₂ Nanoparticles as Biosorbent Material for Methyl Blue Dye Removal from Aqueous Solutions. *Pollution*, 8(1), 295-302.
- Mouni, L., Belkhir, L., Bollinger, J. C., Bouzaza, A., Assadi, A., Tirri, A., ... & Remini, H. (2018). Removal of Methylene Blue from aqueous solutions by adsorption on Kaolin: Kinetic and equilibrium studies. *Applied Clay Science*, 153, 38-45.
- Saeed, T., Naem, A., Din, I. U., Farooq, M., Khan, I. W., Hamayun, M., & Malik, T. (2022). Synthesis of chitosan composite of metal-organic framework for the adsorption of dyes; kinetic and thermodynamic approach. *Journal of Hazardous Materials*, 427, 127902.
- Scatchard, G. D. (1949). The attractions of proteins for small molecules and ions. *Ann. NY Acad. Sci.*, 51, 660-672.
- Song, B., Cao, X., Gao, W., Aziz, S., Gao, S., Lam, C. H., & Lin, R. (2022). Preparation of nano-biochar from conventional biorefineries for high-value applications. *Renewable and Sustainable Energy Reviews*, 157, 112057.
- Srikhaow, A., Chaengsawang, W., Kiatsiriroat, T., Kajitvichyanukul, P., & Smith, S. M. (2022). Adsorption Kinetics of Imidacloprid, Acetamiprid and Methomyl Pesticides in Aqueous Solution onto Eucalyptus Woodchip Derived Biochar. *Minerals*, 12(5), 528.
- Temkin, M. J., & Pyzhev, V. (1940). Recent modifications to Langmuir isotherms.
- Wang, H., Jia, S., Wang, H., Li, B., Liu, W., Li, N., ... & Li, C. Z. (2017). A novel-green biosorbent based on betaine-modified magnetic nanoparticles for removal of methyl blue. *Science Bulletin*, 62(5), 319-325.
- Wang, J., & Wang, S. (2019). Preparation, modification and environmental application of biochar: a review. *Journal of Cleaner Production*, 227, 1002-1022.
- Wang, Y., Zhang, Y., Li, S., Zhong, W., & Wei, W. (2018). Enhanced methylene blue adsorption onto activated reed-derived biochar by tannic acid. *Journal of Molecular Liquids*, 268, 658-666.

- Wong, S., Ngadi, N., Inuwa, I. M., & Hassan, O. (2018). Recent advances in applications of activated carbon from biowaste for wastewater treatment: a short review. *Journal of Cleaner Production*, 175, 361-375.
- Wu, T., Lin, Z., Wu, H., Wang, M., Zhu, C., Kanazawa, N., ... & Liang, R. (2022). Adsorption Studies on Ag (I) Using Poly (N-phenylglycine) Membrane and Application in Practical Silver Recycling. *ACS Applied Polymer Materials*, 4(5), 3333-3342.
- Yagnamurthy, S., Rakshit, D., Jain, S., Rocky, K. A., Islam, M. A., & Saha, B. B. (2022). Adsorption of difluoromethane onto activated carbon based composites: Adsorption kinetics, heat of adsorption, cooling performance and irreversibility evaluation. *Applied Thermal Engineering*, 210, 118359.
- Zhang, H., Tian, S., Zhu, Y., Zhong, W., Qiu, R., & Han, L. (2022). Insight into the adsorption isotherms and kinetics of Pb (II) on pellet biochar via in-situ non-destructive 3D visualization using micro-computed tomography. *Bioresource Technology*, 127406.
- Zhao, F., Fang, S., Gao, Y., & Bi, J. (2022). Removal of aqueous pharmaceuticals by magnetically functionalized Zr-MOFs: Adsorption Kinetics, Isotherms, and regeneration. *Journal of colloid and interface science*, 615, 876-886.

Author Information

Okan Bayram

Department of Chemistry, Graduate School of Applied and Natural Sciences, Suleyman Demirel University, Isparta, Turkey.

Contact e-mail: okan.bayram.32@gmail.com

Elif Koksal

Department of Chemistry, Graduate School of Applied and Natural Sciences, Suleyman Demirel University, Isparta, Turkey.

Emel Moral

Department of Chemistry, Graduate School of Applied and Natural Sciences, Suleyman Demirel University, Isparta, Turkey.

Fethiye Gode

Department of Chemistry, Faculty of Science and Arts, Suleyman Demirel University, Isparta, Turkey.

Erol Pehlivan

Department of Chemical Engineering, Faculty of Engineering and Natural Sciences, Konya Technical University, Konya, Turkey.

To cite this article:

Bayram, O., Koksal, E., Moral E., Gode, F., & Pehlivan, E. (2022). Efficient Decolorization of Anionic Dye (Methyl Blue) by Natural-Based Biosorbent (nano-Magnetic Sophora Japonica Fruit Seed Biochar). *The Eurasia Proceedings of Science, Technology, Engineering & Mathematics (EPSTEM)*, 17, 69-82.